CHALMERS
UNIVERSITY OF TECHNOLOGY

Rubbing and Drawing: Generic Ways to Improve the Thermoelectric Power Factor of Organic Semiconductors?

ADVANCED ELECTRONIC MATERIALS
www.advelectronicmat.de

Rubbing and Drawing: Generic Ways to Improve the Thermoelectric Power Factor of Organic Semiconductors?

Dorothea Scheunemann, Vishnu Vijayakumar, Huiyan Zeng, Pablo Durand, Nicolas Leclerc, Martin Brinkmann, and Martijn Kemerink**

Highly oriented polymer films can show considerable anisotropy in the thermoelectric properties leading to power factors beyond those predicted by the widely obeyed power law linking the thermopower S and the electrical conductivity σ as $S \propto \sigma^{-1/4}$. This has led to encouraging practical results with respect to the electrical conductivity, notwithstanding that the conditions necessary to enhance σ and S simultaneously are less clear. Here, kinetic Monte Carlo simulations are used to study the impact of structural anisotropy on the thermoelectric properties of disordered organic semiconductors. It is found that stretching is a suitable strategy to improve the conductivity along the direction of strain, whereas the effect on the power factor depends on the morphology the polymer crystallizes. In general, crystalline polymers show a simultaneous increase in σ and S which is not the case for amorphous polymers. Moreover, it is shown that the trends resulting from simulations based on variable-range hopping are in good agreement with experiments and can describe the different functional dependencies in the S versus σ behavior of different directions.

1. Introduction

Semiconducting organic materials have attracted increasing interest as thermoelectric (TE) converters in the recent years due to their potentially low fabrication costs and non-toxicity. As in other organic electronic devices, mastering morphology and crystallinity of polymer semiconductors is a necessity to control the performance of organic TEs. One specific case of morphology, which seems to improve both the mechanical and the electrical properties of organic TEs, is the introduction of structural anisotropy. Experimentally this can be induced by orienting the polymer backbones using high-temperature rubbing or tensile drawing. Such highly oriented conducting polymer films can show considerable increases in the electrical conductivity σ along the direction of orientation, whereas the influence on the Seebeck coefficient S is less clear. Experimental studies on iodine-doped PPVs[1] as well as on poly(3,4-ethylenedioxythiophene) polystyrene sulfonate (PEDOT:PSS)[2,3] have found that the thermopower remains practically constant in the direction of orientation, as illustrated in **Figure 1**a for samples based on PEDOT:PSS fibers. In contrast, for thin films based on poly(2,5-bis(3-alkylthiophen-2-yl)thieno[3,2-*b*]thiophene)(PBTTT), recent reports indicate that in-plane anisotropy can simultaneously enhance the thermopower and the electrical conductivity,[4,5] (see Figure 1b), whereas for films of doped polythiophenes it depends on the experimental conditions whether an anisotropy in the thermopower is observed[6] or not.[7]

This experimental divergence is accompanied by a lack of formal understanding. Shklovskii and Efros discussed the anisotropy of hopping conduction by applying the percolation method to the anisotropic situation in germanium subjected to a large uniaxial stress.[8] They argue that in this case, only one critical percolation cluster exists, which determines the transport in all directions. In consequence, the anisotropy in resistivity ρ results from a pre-exponential factor and scales with $\frac{\rho_{zz}}{\rho_{xx}} = \left(\frac{a}{b}\right)^2$ where a and b are the decay length of an ellipsoidal-shaped wave function. The authors did not address the possibility of anisotropy in the thermopower.

Recently, Vijayakumar et al. experimentally studied the anisotropy in the thermoelectric properties of highly oriented films

Dr. D. Scheunemann
Department of Chemistry and Chemical Engineering
Chalmers University of Technology
Göteborg 41296, Sweden
E-mail: dorsche@chalmers.se
Dr. D. Scheunemann, Prof. M. Kemerink
Complex Materials and Devices
Department of Physics, Chemistry and Biology (IFM)
Linköping University
Linköping 58183, Sweden
Dr. V. Vijayakumar, H. Zeng, Dr. M. Brinkmann
Université de Strasbourg, CNRS
ICS UPR 22, Strasbourg F-67000, France
P. Durand, Dr. N. Leclerc
Université de Strasbourg, CNRS
ICPEES UMR 7515, Strasbourg F-67087, France
Prof. M. Kemerink
Centre for Advanced Materials
Heidelberg University
Im Neuenheimer Feld 225, Heidelberg 69120, Germany
E-mail: martijn.kemerink@cam.uni-heidelberg.de
The ORCID identification number(s) for the author(s) of this article can be found under https://doi.org/10.1002/aelm.202000218.

DOI: 10.1002/aelm.202000218

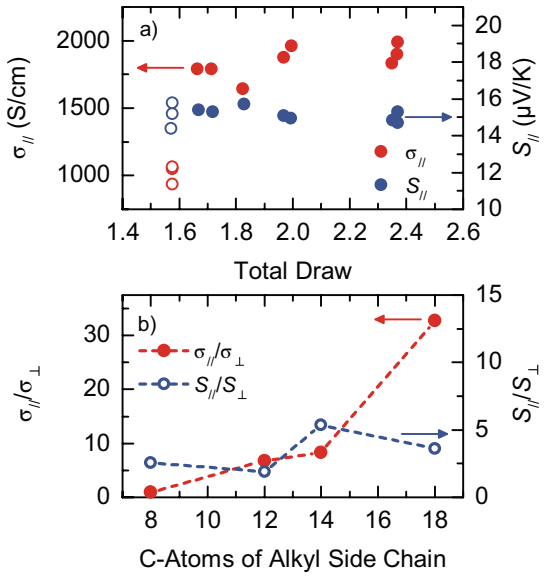

Figure 1. a) Electrical conductivity (red circles) and thermopower (blue circles) of PEDOT:PSS fibers as a function of draw. PEDOT:PSS fibers were spun into 10 vol% DMSO in IPA (open circles) and a fraction of samples was subsequently drawn through a DMSO bath (filled circles). Adapted with permission.[3] Copyright 2019, American Chemical Society. b) Experimental data on PBTTT from ref. [5] showing the anisotropy of the electrical conductivity and thermopower as a function of the alkyl side chain length at a doping time of 6 min. Adapted with permission. Copyright 2019, American Chemical Society.

based on PBTTT and P3HT, respectively.[4] Based on different functional dependencies of $S(\sigma)$ in the different directions, the authors concluded that two different charge transport behaviors may govern the parallel and perpendicular directions. However, this contrasts the interpretation of ref. [7] where for stretched P3HT the same transport mechanism is assumed in all directions. Hence, it is currently not evident how structural anisotropy is influencing the thermoelectric properties of disordered organic semiconductors.

Here, we combined kinetic Monte Carlo (kMC) simulations with conductivity and thermopower measurements on doped PBTTT films to rationalize the impact of anisotropy on the thermoelectric properties of disordered organic semiconductors. We find that variable-range hopping (VRH) can not only consistently describe charge and energy transport in both the parallel and the perpendicular direction but also the trends observed with polymer side chain length. Furthermore, we clarify why some materials show a simultaneous enhancement in conductivity and thermopower in the direction of orientation, whereas for others the Seebeck coefficient remains largely unaffected.

2. Theoretical Framework

The kMC model has been extensively described before.[9,10] In brief, the kMC simulations within this work account for variable-range hopping on a regular or irregular (random) lattice with a mean inter-site distance of $a_{NN} = N_0^{-1/3} = 1.8$ nm with N_0 the total site density. Site energies are distributed according to an exponential density of states (DOS) with varying degree of disorder. An exponential form is chosen to reflect the doping-induced DOS tail that forms irrespective of the, typically Gaussian, shape of the undoped material.[11,12] Only on-site Coulomb interactions between mobile charges are accounted for. In contrast to the approach where full Coulomb interactions (charge–charge and charge–dopant) are accounted for, as previously used to describe doping,[12,13] the current approach allows to keep calculation times reasonable, that is, hours to days on a fast pc. Hopping probabilities are calculated from a Miller–Abrahams type expression,[14] while anisotropy is introduced via the localization length. Polaronic effects in terms of Marcus theory were not explicitly taken into account as we have thus far been able to describe experimental data without explicitly accounting for polaronic effects using the simpler Miller–Abrahams rates.[12] Similar conclusions regarding the minor differences between the two rates were also drawn by Mendels and Tessler[15] and Cottaar et al.[16] The electronic contribution to the thermal conductivity was determined as detailed in ref. [17]. For the simulations below, a standard parameter set with an attempt to hop frequency $\nu_0 = 10^{13}\,s^{-1}$, an exponential disorder of $\sigma_{DOS} = 4\ k_B T$, an inter-site distance of $a_{NN} = 1.8$ nm, a localization length of $\alpha = \alpha_0 \cdot [\alpha_{xy}\,\alpha_{xy}\,\alpha_z] = 0.4 \cdot [112]$ nm a relative concentration $c = \frac{n}{N_0} = 0.01$ with n the absolute charge carrier concentration and z being the direction of strain, a temperature $T = 300$ K, a dielectric constant of $\varepsilon_r = 2.7$, and a regular lattice is used unless indicated otherwise. The critical percolation network is illustrated by adding connections between sites in the order of their respective inter-site transition rates as determined from the Miller–Abrahams rates. Connections are added to the network until a set of connected bonds forms a subnetwork that spans the full simulation box in the direction in which the conductivity is probed.

3. Results

In polymer films, the crystallization behavior, which has a major impact on nanomorphology, is often a key issue with respect to performance control. Therefore, we discuss first the influence of structural differences in terms of different lattice structures. The upper panel of **Figure 2**a shows the anisotropy of conductivity and thermopower as a function of the anisotropy ratio $\alpha_\parallel/\alpha_\perp$ for a random lattice. We find that this type of lattice results in a thermopower, which is independent on the direction of transport, while the anisotropy in conductivity scales quadratic with the anisotropy ratio, as predicted by Efros und Shklovskii.[8] In agreement with their assumption, the critical percolation network for this case is found to be similar in all directions of transport as depicted in Figure 2b and also similar to the isotropic case (see Figure 2c). This is also reflected in the percolation threshold, here defined as the minimum number of bonds required until a path in the respective direction is formed. As shown in the lower panel of Figure 2a, this number is independent of the direction of transport, which correlates with the behavior of the transport energy and a thermopower that is independent on the direction of transport.

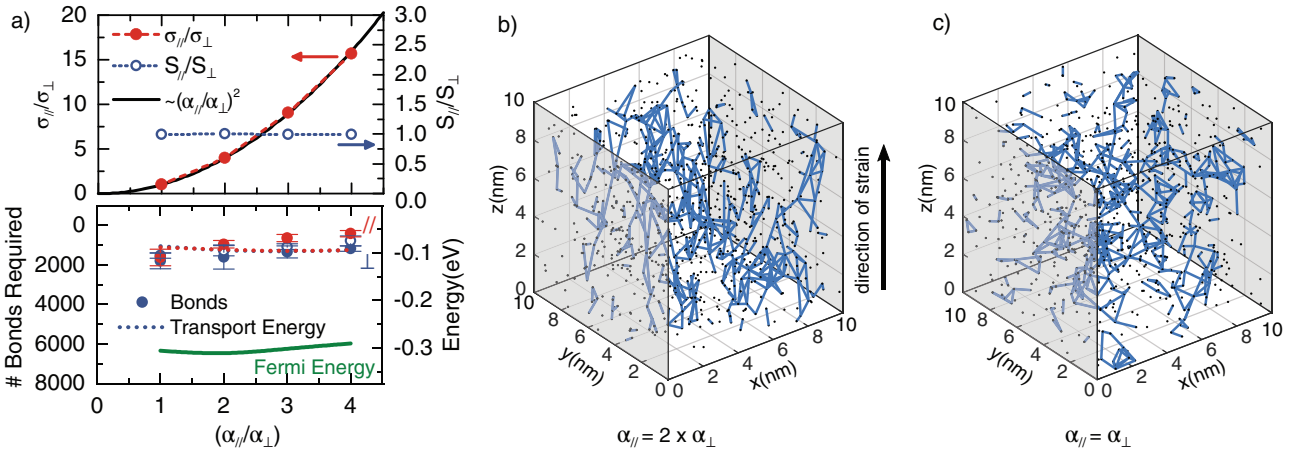

Figure 2. Hopping on a random lattice at a relative carrier concentration of $c = 0.01$. a) Anisotropy in electrical conductivity $\sigma_{\parallel}/\sigma_{\perp}$ (filled red circles) and Seebeck coefficient $S_{\parallel}/S_{\perp}$ (open blue circles) (upper panel) and minimum number of bonds required until a path in the respective direction is reached (symbols) (lower panel) as a function of the anisotropy ratio. The dotted lines in the lower panel present the transport energy E_{tr} for the parallel (red) and perpendicular (blue) direction, respectively. The green line represents the Fermi energy E_F. b,c) Critical percolation cluster (blue lines) for hopping on a random lattice with $\alpha = 0.4 \cdot [112]$ nm (b) and $\alpha = 0.4 \cdot [111]$ nm (c). Black dots represent available sites; gray surfaces indicate the yz-planes.

In contrast, for a regular lattice, the critical percolation network has a distinct orientation in the direction of strain, (see **Figure 3**b) and clearly differs from the percolation network for the isotropic case (see Figure 3c). This results in an anisotropy in the thermopower, which is increasing with anisotropy ratio and an anisotropy in conductivity that scales roughly exponentially with the anisotropy ratio, as depicted in Figure 3a. Qualitatively, the observed behavior can be understood as follows: The thermopower is given by $S \propto (E_F - E_{tr})/T$ with E_F the Fermi energy, E_{tr} the transport energy, and T the temperature and therefore a direct measure of the energy difference $\Delta E = E_F - E_{tr}$. For a highly anisotropic localization radius that is small compared to the nearest neighbor distance on a regular lattice, carriers are "forced" to hop along the parallel direction and therefore have a reduced ability to optimize their path with respect to energy. This leads to the highly anisotropic percolating network as depicted in Figure 3b, and a percolation threshold that is reduced in the parallel compared to the perpendicular direction and concomitantly an upward shift of the transport energy in this direction, as depicted in the lower panel of Figure 3a. Finally, this results in an increase in $S_{\parallel}$ compared to $S_{\perp}$. In consequence, the introduction of structural anisotropy enhances the power factor $PF = \sigma S^2$ in the parallel direction, as also observed experimentally for aligned PBTTT and P3HT films.[4–6] As depicted in Figure S1, Supporting Information, this enhancement is especially pronounced for the case of a regular lattice. Additionally, we would like to note that the introduction of structural anisotropy also results in an anisotropy in the electronic contribution to the thermal conductivity as depicted in Figure S2, Supporting Information. However, we showed in

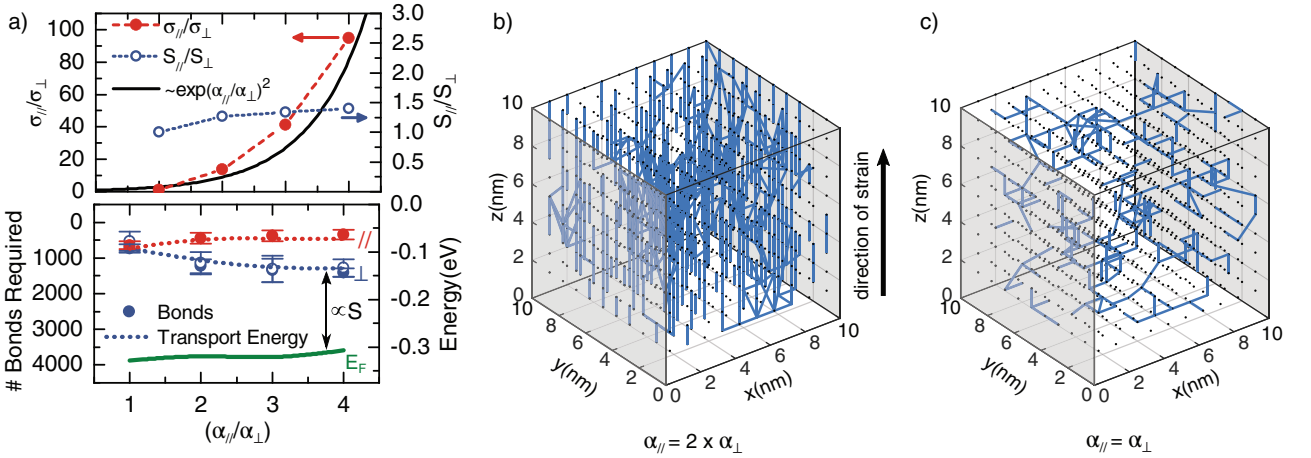

Figure 3. Hopping on a regular lattice at a relative carrier concentration of $c = 0.01$. a) Anisotropy in electrical conductivity $\sigma_{\parallel}/\sigma_{\perp}$ (filled red circles) and Seebeck coefficient $S_{\parallel}/S_{\perp}$ (open blue circles) (upper panel) and minimum number of bonds required until a path in the respective direction is reached (symbols) (lower panel) as a function of the anisotropy ratio. The dotted lines in the lower panel present the transport energy E_{tr} for the parallel (red) and perpendicular (blue) direction, respectively. The green line represents the Fermi energy E_F. b,c) Critical percolation cluster (blue lines) for hopping on a regular lattice with $\alpha = 0.4 \cdot [112]$ nm (b) and $\alpha = 0.4 \cdot [111]$ nm (c). Black dots represent available sites; gray surfaces indicate the yz-planes.

a recent article[17] that for most systems reported to date the lattice contribution is dominating the thermal conductivity.

The investigations above clarify the diverging results observed experimentally for the anisotropy of the thermopower. For more amorphous polymers like PEDOT:PSS, a random lattice can reasonably be assumed.[18,19] In the simulations above, this assumption adequately reproduces the experimental finding of an isotropic thermopower shown in refs. [2,3] and also the correlation of hopping length in parallel and perpendicular direction to conductivity in these directions found by Nardes et al.[18] In contrast, highly crystalline polymers like PBTTT show strong spatial correlations and therefore are not random systems. Hence, the anisotropy in thermopower must, in first order, be described using a regular lattice. Whether semicrystalline polymers like P3HT can be classified to one or the other group will likely depend on the preparation conditions and the corresponding degree of crystallinity.

To test the predictions of the model on real devices, we used thin films based on a series of doped PBTTT polymers that differ by the length of their alkyl side chains, from n-octyl to n-dodecyl (C_8, C_{12}). A short summary of the experiments is given in the methods section, for full details we refer to refs. [6, 20, 21]. **Figure 4** shows the experimentally determined conductivity dependence of the thermopower and power factor together with the results of the kMC simulations. In the perpendicular direction, the experimentally determined thermopower follow a universal curve, independent of the polymer or the dopant used. This is not the case for the parallel direction.

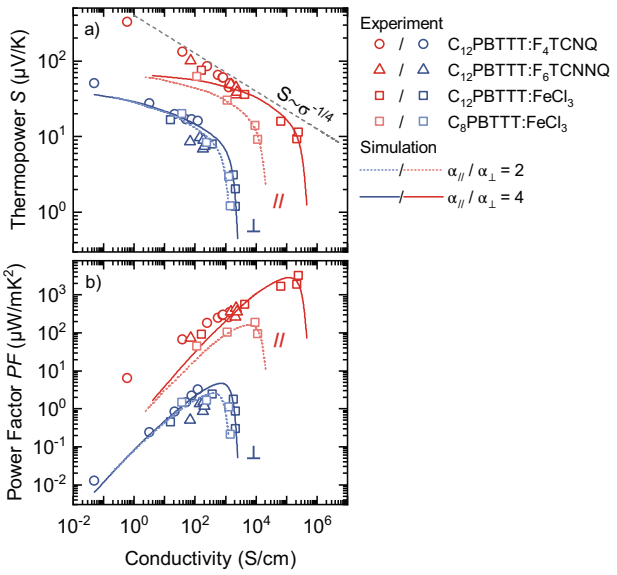

Figure 4. a) Thermopower S and b) power factor PF versus conductivity of highly oriented thin films based on C_8PBTTT doped with $FeCl_3$ (bright squares) and C_{12}PBTTT doped with F_4TCNQ (circles), F_6TCNNQ (triangles), and $FeCl_3$ (squares). Lines correspond to simulations calculated from the kMC model applied to a regular lattice, with an attempt to hop frequency of $\nu_0 = 3 \times 10^{14}\,s^{-1}$ and a thermopower rescaled by a factor of 0.05 (0.075) in the perpendicular (parallel) direction. Dotted lines represent an anisotropy ratio of $\alpha_{\parallel}/\alpha_{\perp} = 2$, whereas full lines show the result for an anisotropy ratio of $\alpha_{\parallel}/\alpha_{\perp} = 4$. $\parallel$ and $\perp$ refer to the parallel and perpendicular direction, respectively. The dashed gray line shows the –1/4 power-law relationship observed experimentally.

Here, the experimental data follow at lower conductivities the "universal" –1/4 power-law relationship that was previously noted by Glaudell et al.[22] and explained by Abdalla et al.[12] but show a roll-off that depends on the length of the alkyl side chain. Tanaka et al.[23] recently interpreted a similar roll-off and the correspondent maximum in the PF in terms of a transition from non-metallic to metallic behavior in highly doped PBTTT, reflecting a change in localization. Figure 4 shows that phenomenologically the same behavior can be obtained from a system with constant localization. Both the trend in the perpendicular and the parallel direction can be well reproduced by our kMC model (lines), when assuming that the anisotropy ratio is varied from $\alpha_{\parallel}/\alpha_{\perp} = 2$ (dotted lines) to $\alpha_{\parallel}/\alpha_{\perp} = 4$ (full lines). This increase in the anisotropy ratio $\alpha_{\parallel}/\alpha_{\perp}$ enhances the anisotropy in conductivity and thermopower, in accordance with the results shown in Figure 3a. The assumption of a variation in anisotropy ratio with alkyl side chain length of the polymer is reasonable, when considering that the rubbed films consist mainly of aligned face-on oriented crystals and the interlayer spacing increases with alkyl side chain length.[5] Detailed investigations on how the polymer structure relates to the anisotropy factor will be the topic of further research. We attribute the fact that the experimentally observed –1/4 power-law relationship is not well reproduced by the kMC simulations to the approximate treatment of the Coulomb interaction, as discussed in Section 2; in ref. [13], it is shown that a more realistic DOS shape in an otherwise similar model does reproduces the –1/4 power-law relationship.

To scale the absolute values, the attempt to hop frequency ν_0 was set to a value of $\nu_0 = 3 \times 10^{14}\,s^{-1}$, whereas the thermopower was rescaled by a factor of 0.05 (0.075) in the perpendicular (parallel) direction. The latter indicates that the kMC model is not perfectly adjusted on an absolute energy scale, implying that disorder is most likely overestimated. A more quantitative description will be in the focus of upcoming work. However, the model is able to capture the qualitative behavior of the data, without the need to assume different transport mechanisms in the in- and out-of-plane directions.

Figure 5 shows the anisotropy in the S versus σ relation with respect to the localization length prefactor α_0. Increasing the overall localization length results in an increase in conductivity as could be expected for a stronger wavefunction overlap between adjacent sides. At the same time, anisotropy in both σ and S is reduced with increasing α_0 as illustrated in Figure 5b,c. Once the actual tunneling distances, that scale with α, get larger than the typical inter-site distance, the effect of the correlations in the (regular) lattice gets washed out. Equivalently, the effect of increasing α_0 may be understood as making the system behave more like a true VRH system with significant hopping to non-nearest sites for which only a mild anisotropy in conductivity, but not in thermopower, is observed (c.f. Figure 2). The exact value of the anisotropy depends moreover on the energetic disorder σ_{DOS}. Specifically, increasing the energetic disorder decreases the anisotropy in the conductivity (see Figure 5b) but at the same time increases the anisotropy in the thermopower (see Figure 5c). However, with respect to high power factors $PF = S^2\sigma$, a low energetic disorder is preferential as this leads to an increase in the absolute value of the conductivity that is higher than the decrease in S^2.

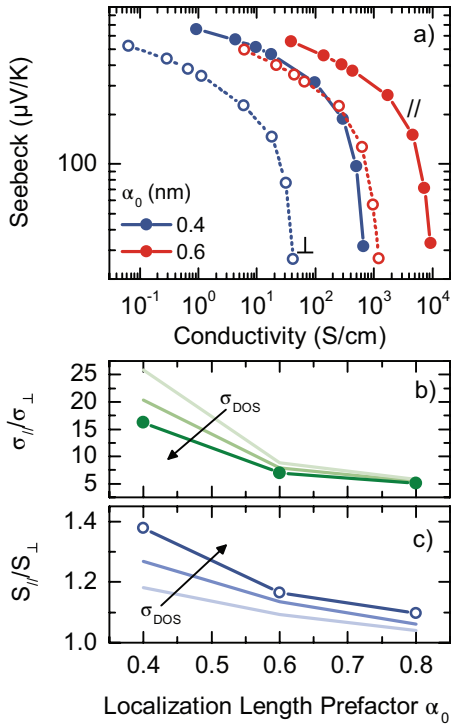

Figure 5. a) Simulated thermopower S as a function of the electrical conductivity σ for a regular lattice with different localization length prefactors α_0. ∥ (filled circles) and ⊥ (open circles) refer to the parallel and perpendicular directions, respectively. b,c) Anisotropy in electrical conductivity $\sigma_{\parallel}/\sigma_{\perp}$ (b) and Seebeck coefficient $S_{\parallel}/S_{\perp}$ (c) in the parallel and perpendicular direction as a function of the localization length prefactor α_0 and for a variation of the energetic disorder σ_{DOS}, ranging from $\sigma_{DOS} = 2\,k_BT$ to $4\,k_BT$, $\alpha = \alpha_0 \cdot$ [112].

4. Conclusion

With the help of kinetic Monte Carlo simulations, we systematically investigated the impact of structural anisotropy in disordered organic semiconductors. By analyzing the impact of the parameters affecting the length scales and the structural order of such systems, we examine under which conditions creating structural anisotropy by, for example, rubbing or drawing, is a suitable strategy to enhance the power factor of organic thermoelectric materials.

Even though the quantitative relation between "stretching" and the absolute values of the localization length is not clear, we could show here that qualitative agreement with key experimental observations can be obtained by introducing structural anisotropy via an increase of the localization length in the parallel direction and keeping $\alpha_{\perp}$ constant. In contrast, an approach that keeps the sum or the product of $\alpha_{\perp}$ and $\alpha_{\parallel}$ constant leads to a decrease in $\sigma_{\perp}$, which is not observed in experiments.

Furthermore, we showed that well known strategies, such as aiming for low energetic disorder and high localization length which lead in general to high power factors, are also the method of choice in the case of structural anisotropy. However, structural anisotropy offers an additional tool. On the one hand, the power factor (in parallel direction) can be further increased compared to the isotropic case as the commonly observed trade-off between conductivity increase and thermopower decrease can be avoided, and power factors beyond values predicted by the empirical power law $S \propto \sigma^{-1/4}$ can be achieved. Particularly promising in this context are highly crystalline polymers, corresponding to a regular hopping lattice in our model, that allow a simultaneous, anisotropy-induced increase in the thermopower and conductivity and therefore the highest power factors. On the other hand, the use of structural anisotropy offers an alternative to increasing the overall localization length, since when using a highly crystalline material, increasing α in one direction by stretching leads to similarly high power factors in that direction as increasing the overall α would do. Technically, this can be advantageous, since methods to create structural anisotropy in polymer films are well known,[24–26] whereas it may be more difficult to increase the overall localization length.

5. Experimental Section

C_8PBTTT (M_w = 24 000 g mol^{-1}, M_n = 13 000 g mol^{-1}) and C_{12}PBTTT (M_w = 45 000 g mol^{-1}, M_n = 26 000 g mol^{-1}) were synthesized according to the synthetic path given in refs. [4,5]. The F_6TCNNQ dopant was synthesized following ref. [20]. High-temperature rubbing of PBTTT films was performed using the protocol defined in refs. [6, 24]. 30–60 nm thick polymer films were rubbed at 125 °C on a sacrificial layer of NaPSS on clean glass substrates. The alignment was quantified by polarized UV–vis–NIR spectroscopy using a Cary 5000 spectrometer. The aligned PBTTT films were floated on distilled water and recovered on pre-patterned glass substrates for four-point conductivity and Seebeck coefficient measurements.[6] The deposition of gold contacts and the geometry of the electrode patterns are described in ref. [6]. Sequential doping was performed in a Jacomex glovebox (p_{O_2} < 1 ppm and p_{H_2O} < 1 ppm) using anhydrous acetonitrile (F_4TCNQ and F_6TCNNQ) and nitromethane ($FeCl_3$) following the protocol described in ref. [4]. All solvents were used as received from Sigma-Aldrich. Charge conductivity and Seebeck coefficients were probed using a Keithley 4200 source meter and a Lab Assistant Semi-Probe station along and perpendicular to the rubbing directions just after doping (to avoid aging of the samples).[4,5] Additional experimental details can be found in a forthcoming publication.[21]

Supporting Information

Supporting Information is available from the Wiley Online Library or from the author.

Acknowledgements

D.S. acknowledges funding through the European Union's Horizon 2020 research and innovation program under the Marie Skłodowska-Curie grant agreement No 799477. Financial supports from the ANR Anisotherm (ANR-17-CE05-0012) and CNRS grant PEPS Thermobody are gratefully acknowledged.

Conflict of Interest

The authors declare no conflict of interest.

Keywords

charge transport, conjugated polymers, kinetic Monte Carlo simulations, morphology, organic thermoelectrics, Seebeck coefficient

Received: February 28, 2020
Revised: April 24, 2020
Published online: July 14, 2020

[1] Y. Hiroshige, M. Ookawa, N. Toshima, *Synth. Met.* **2006**, *156*, 1341.
[2] Q. Wei, M. Mukaida, K. Kirihara, T. Ishida, *ACS Macro Lett.* **2014**, *3*, 948.
[3] R. Sarabia-Riquelme, M. Shahi, J. W. Brill, M. C. Weisenberger, *ACS Appl. Polym. Mater.* **2019**, *1*, 2157.
[4] V. Vijayakumar, Y. Zhong, V. Untilova, M. Bahri, L. Herrmann, L. Biniek, N. Leclerc, M. Brinkmann, *Adv. Energy Mater.* **2019**, *9*, 1900266.
[5] V. Vijayakumar, E. Zaborova, L. Biniek, H. Zeng, L. Herrmann, A. Carvalho, O. Boyron, N. Leclerc, M. Brinkmann, *ACS Appl. Mater. Interfaces* **2019**, *11*, 4942.
[6] A. Hamidi-Sakr, L. Biniek, J.-L. Bantignies, D. Maurin, L. Herrmann, N. Leclerc, P. Lévêque, V. Vijayakumar, N. Zimmermann, M. Brinkmann, *Adv. Funct. Mater.* **2017**, *27*, 1700173.
[7] J. Hynynen, E. Järsvall, R. Kroon, Y. Zhang, S. Barlow, S. R. Marder, M. Kemerink, A. Lund, C. Müller, *ACS Macro Lett.* **2019**, *8*, 70.
[8] B. I. Shklovskii, A. L. Efros, *Electronic Properties of Doped Semiconductors*, Springer-Verlag, Berlin **1984**.
[9] H. Abdalla, K. van de Ruit, M. Kemerink, *Sci. Rep.* **2015**, *5*, 16870.
[10] G. Zuo, H. Abdalla, M. Kemerink, *Adv. Electron. Mater.* **2019**, *0*, 1800821.
[11] M. Silver, L. Pautmeier, H. Bässler, *Solid State Commun.* **1989**, *72*, 177.
[12] H. Abdalla, G. Zuo, M. Kemerink, *Phys. Rev. B* **2017**, *96*, 241202.
[13] C. J. Boyle, M. Upadhyaya, P. Wang, L. A. Renna, M. Lu-Díaz, S. Pyo Jeong, N. Hight-Huf, L. Korugic-Karasz, M. D. Barnes, Z. Aksamija, D. Venkataraman, *Nat. Commun.* **2019**, *10*, 2827.
[14] A. Miller, E. Abrahams, *Phys. Rev.* **1960**, *120*, 745.
[15] D. Mendels, N. Tessler, *J. Phys. Chem. Lett.* **2014**, *5*, 3247.
[16] J. Cottaar, R. Coehoorn, P. A. Bobbert, *Phys. Rev. B* **2012**, *85*, 245205.
[17] D. Scheunemann, M. Kemerink, *Phys. Rev. B* **2020**, *101*, 075206.
[18] A. M. Nardes, M. Kemerink, R. A. J. Janssen, *Phys. Rev. B* **2007**, *76*, 085208.
[19] L. Ouyang, C. Musumeci, M. J. Jafari, T. Ederth, O. Inganäs, *ACS Appl. Mater. Interfaces* **2015**, *7*, 19764.
[20] P. K. Koech, A. B. Padmaperuma, L. Wang, J. S. Swensen, E. Polikarpov, J. T. Darsell, J. E. Rainbolt, D. J. Gaspar, *Chem. Mater.* **2010**, *22*, 3926.
[21] V. Vijayakumar, P. Durand, H. Zeng, V. Untilova, L. Herrmann, P. Algayer, N. Leclerc, M. Brinkmann, unpublished.
[22] A. M. Glaudell, J. E. Cochran, S. N. Patel, M. L. Chabinyc, *Adv. Energy Mater.* **2015**, *5*, 1401072.
[23] H. Tanaka, K. Kanahashi, N. Takekoshi, H. Mada, H. Ito, H. Shimoi, Y. Ohta, T. Takenobu, *Sci. Adv.* **2020**, *6*, eaay8065.
[24] L. Biniek, S. Pouget, D. Djurado, E. Gonthier, K. Tremel, N. Kayunkid, E. Zaborova, N. Crespo-Monteiro, O. Boyron, N. Leclerc, S. Ludwigs, M. Brinkmann, *Macromolecules* **2014**, *47*, 3871.
[25] M. Brinkmann, L. Hartmann, L. Biniek, K. Tremel, N. Kayunkid, *Macromol. Rapid Commun.* **2014**, *35*, 9.
[26] M. Pandey, N. Kumari, S. Nagamatsu, S. S. Pandey, *J. Mater. Chem. C* **2019**, *7*, 13323.